Transparent and Cell-Guiding Cellulose Nanofiber 3D Printing Bioinks

Radeke, Carmen; Pons, Raphaël; Mihajlovic, Marko; Knudsen, Jonas R.; Butdayev, Sarkhan; Kempen, Paul J.; Segeritz, Charis Patricia; Andresen, Thomas L.; Pehmøller, Christian K.; Jensen, Thomas E.

Total number of authors:
11

Published in:
ACS Applied Materials and Interfaces

Link to article, DOI:
10.1021/acsami.2c16126

Publication date:
2023

Document Version
Peer reviewed version

Transparent and cell-guiding cellulose nanofiber 3D printing bioinks

Carmen Radeke[1], Raphaël Pons[1], Marko Mihajlovic[1], Jonas R. Knudsen[3,4], Sarkhan Butdayev[1], Paul Kempen[1,2], Charis-Patricia Segeritz[4], Thomas L. Andresen[1], Christian K. Pehmøller[4], Thomas E. Jensen[3], and Johan U. Lind[1,]*

[1] Department of Health Technology, Technical University of Denmark, 2800 Kgs. Lyngby, DK-Denmark

[2] The National Center for Nano Fabrication and Characterization, DTU Nanolab, Technical University of Denmark, 2800 Kgs. Lyngby, DK-Denmark

[3] August Krogh Section for Molecular Physiology, Department of Nutrition, Exercise and Sports, Faculty of Science, University of Copenhagen, 2100 Copenhagen, Denmark

[4] Heart and Skeletal Muscle Biology, Global Drug Discovery, Novo Nordisk A/S, 2760 Maaloev, Denmark

[*] Corresponding author: joli@dtu.dk

KEYWORDS Extrusion-based bioprinting, Nanofibrillated cellulose, Carboxymethylation

Skeletal muscle, Tissue models

ABSTRACT

For 3D bioprinting to fulfill its promise and enable automated fabrication of complex tissue-mimicking constructs, there is a need for developing bioinks that are not only printable and biocompatible, but also have integrated cell-instructive properties. Towards this goal, we here present a scalable technique for generating nanofiber 3D printing inks with unique tissue-guiding capabilities. Our core methodology relies on tailoring the size and dispersibility of cellulose fibrils, through a solvent-controlled partial carboxymethylation. This way, we generate partially negatively charged cellulose nanofibers with diameters of ~250 nm and lengths spanning tens to hundreds of microns. In this range, the fibers structurally match the size and dimensions of natural collagen fibers making them sufficiently large to orient cells. Yet, they are simultaneously sufficiently thin to be optically transparent. By adjusting fiber concentration, 3D printing inks with excellent shear thinning properties can be established. In addition, as the fibers are readily dispersible, composite inks with both carbohydrates and ECM-derived proteins can easily be generated. We apply such composite inks for 3D printing cell-laden and cross-linkable structures, as well as tissue-guiding gel substrates. Interestingly, we find that the spatial organization of engineered tissues can be defined by the shear-induced alignment of fibers during the printing procedure. Specifically, we show how myotubes derived from human and murine skeletal myoblasts can be programmed into linear and complex non-linear architectures on soft printed substrates with intermediate fiber contents. Our nanofibrillated cellulose inks can thus serve as a simple and scalable tool for engineering anisotropic human muscle tissues that mimic native structure and function.

INTRODUCTION

Extrusion-based three-dimensional (3D) printing is redefining *in vitro* and *in vivo* biomedical research, by enabling automated fabrication of complex biomaterial scaffolds[1], engineered tissues[2], and micro-physiological systems[3]. Across these areas, a core challenge in 3D bioprinting is the formulation of biomaterial inks that facilitate the formation of functional tissues from embedded cells or spheroids, while simultaneously assuring printability and shape-fidelity[4,5]. Bioinks incorporating nano- and micro-fibrils are intriguing in both of these regards. In the first regard, fibrillar inks may structurally mimic extracellular matrix (ECM) nanofibers derived from e.g. collagen and fibronectin that guide cellular adhesion, migration, proliferation, differentiation and organization in the native tissue[6]. In the second regard, fibrillary components can be potent thixotropic agents at low concentrations, capable of forming viscous shear-thinning solutions or viscoelastic gels with low yield stress for extrusion-based printing[7–11].

Two diverse approaches currently coexist within fibrillary bioinks: The most widespread approach relies on simply applying ECM-derived biomaterials as the core component of the inks. Here, nanofiber polymerization generally occurs after deposition, and often lead to the formation of viscoelastic gels. Common examples are collagen where a post-printing temperature increase to physiological levels induces polymerization of soluble collagen into fibers, or fibrin where thrombin is applied to induce polymerization of fibrinogen to fibrin[12]. Similarly, for inks based on decellularized ECM (dECM) derived from primary tissues or in the form of commercial Matrigel®, gel formation is induced by ECM fiber polymerization in response to physiological temperature[13,14]. The other key direction within nanofibrillar inks relies on producing micro- or nano-fibrils prior to ink formulation and printing. In these cases, the fibrils simultaneously serve as rheological modifiers, ensuring reliable extrusion or multilayer stacking[7]. Various types of

nano- and micro-fibrils have been introduced, including fibrils derived from collagen[15], modified hyaluronic acid[16], mechanically fractured electrospun polymers such as polycaprolactone (PCL)[17], and cellulose nanofibers[7–11].

Cellulose nanomaterials and nanofibers are highly diverse, and nomenclature often inconsistent. They span from tiny cellulose nanocrystals (CNC) with diameters ~2-20 nm and lengths of 100-600 nm to microfibrillated cellulose (MFC) where diameters span from the nano- to micro-range, but where lengths are generally much longer than 1 μm. Nanofibrillated cellulose (NFC) usually refer to fibrils with lengths similar to MFC (>>1 μm), but where diameter are consistently below 1 μm. Regardless of inconsistencies in nomenclature, CNC, NFC, and MFC have all been applied in a range of 3D printing applications as they all can display shear-thinning behavior, biocompatibility, and low cost. [7,18–22] Early on, biomimetic 3D structures such as a human ear were for instance been printed by combining MFC with alginate, followed by ionic cross-linking.[7] However, a key challenge for MFC-derived inks is the limited transparency caused by light diffraction by the larger fibers and aggregates. This is particularly problematic for cell and tissue engineering applications where optical microscopy is an essential tool. One potential solution is to degrade the cellulose using e.g. chemical oxidation. For instance, oxidization of fibrillary cellulose using 2,2,6,6-tetramethylpyperidine-1-oxyl (TEMPO) yields transparent gel with shear-thinning rheological properties[9–11,23,24]. This approach have been applied to yield bioprinting inks that e.g. incorporate gelatin to provide cell adhesive motifs [10,11]. However, TEMPO oxidation of NFC generally yields fibers in the single micron range or less[25,26], far shorter than single collagen fibers that range between 20-200 μm.[27] This compromises ability of such highly degraded cellulose fibers for guiding tissue organization.

As an alternative to such procedures, we here present a robust protocol for generating optically transparent MFC inks that retain lengths of tens to several hundred microns. Specifically, we tailored the well-known carboxymethylation reaction[28–31] to partially functionalize and oxidize MFC. Thereby we generated transparent fibers with widths in the range of a few hundred of nanometers, just below the wavelength of visible light. In tuning the reaction, we found that adjusting the polarity of mixed alcohol reaction solvent is effective in controlling the degree of reaction. The partially carboxymethylated nanofibrillated cellulose (cNFC) readily disperse in aqueous buffers, but display less pronounced shear-thinning properties that the non-treated MFC counterparts. However, we found that excellent printability can be reestablished by increasing cNFC concentration slightly. The cNFC is further readily miscible with protein biomaterials, such as gelatin and collagen, which we leveraged to create cell-adhesive composite bioprinting inks. Interestingly, these composite inks can serve as programmable biomaterial scaffolds for aligning skeletal muscle myotubes derived from human or murine myoblasts. Replicating the native alignment of skeletal myotubes has been found beneficial for generating in vitro tissue models with physio-mimetic myotube lengths and function[32–37]. When cultured on planar, printed cNFC:gelatin composites, myotube extension follows print direction, in accordance with shear-induced orientation of the embedded fibers during extrusion. We demonstrate the robustness of our procedure by organizing muscle tissues into a range of anisotropic, linear, and complex architectures. The cNFC-based inks are thus promising as a scalable material for generating physiologically relevant models of striated muscle.

RESULTS

As our base material, we applied a commercially available aqueous MFC paste, which was generated from wood pulp cellulose by mechanical shearing. Without further modifications, the MFC was readily printable from concentrations ≥1% w/v with a characteristic white appearance, indicative of fibers and aggregates scattering visible light. To improve material transparency, we chose carboxymethylation, which has previously been applied to generate transparent MFC[30,31]. However, similarly to cellulose nanofibrils generated using TEMPO oxidation, reported transparent carboxymethylated fibers have diameters <20 nm and lengths ~1µm, limiting their structural similarity to ECM protein nanofibers[21,22,30]. To gain transparency while retaining structural properties, we here aimed to generate fibrils with diameters just below the wavelength of visible light.

To control the degree of carboxymethylation, we investigated the effect of adjusting solvent composition in detail. In addition to amount of reactants, solvents have previously been shown to influence the overall degree of reaction[29] in bulk cellulose treatments. In general, the reaction comprised two steps: *i)* Dispersing a stock MFC aqueous paste (10% w/v) in polar organic solvent for mercerization with sodium hydroxide (NaOH), *ii)* etherification with monochloroacetic acid (MCA), see figure 1a. For the majority of our studies the amount of reactants relative to cellulose anhydroglucose units (AGU) were 2.5:1 NaOH:AGU and 1:1 MCA:AGU. To evaluate the degree of reaction we applied Fourier transformed-infrared spectroscopy (FT-IR) and quantified the relative degree of substitution (DS_{rel}) by relating the stretching vibration of the carboxylate peak at 1595 cm^{-1} to the stretching vibration of the C-H group at 2894 cm^{-1}, similarly to Miyamoto *et al.*[38]

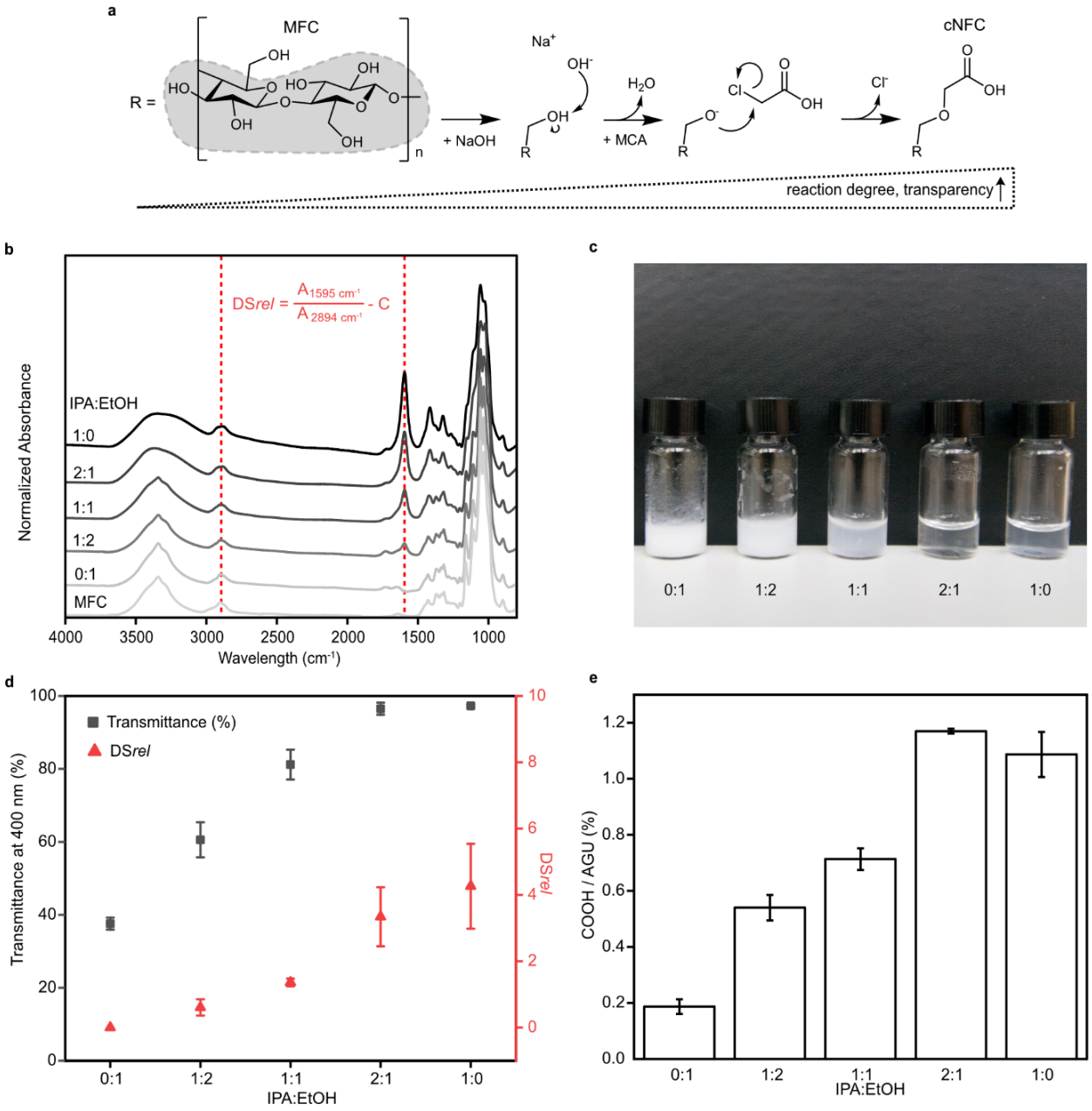

Figure 1. Carboxymethylation of MFC in different solvents compositions: comparison of DS_{rel} and transmittance. (a) Reaction mechanism of carboxymethylation of MFC. Increasing the degree of reaction increases transparency of substituted fibers. (b) FT-IR of MFC reacted in 0:1, 1:2, 1:1, 2:1, and 1:0 IPA:EtOH. Normalized absorbance used to calculate degree of substitution (rel). (c) Photograph of fibers reacted in respective IPA:EtOH mixes at 2.5:1 NaOH:AGU/1:1 MCA:AGU. (d) Transmittance at 400 nm in % and DS_{rel} calculated based on IR data of 2.5:1 NaOH:AGU/1:1

MCA:AGU. Full transmission spectra across UV-VIS region can be found in supplementary information (e) Degree of substitution calculated by titration of fibers. Error-bars indicate standard error of the mean (SEM) for n=3.

We initially screened common polar alcohols including methanol (MeOH), ethanol (EtOH), and isopropanol (IPA). Only in the least polar alcohol –IPA– did we observe a notable carboxylate peak, indicative of a successful reaction (Figure S1). We therefore hypothesized that the degree of reaction may be tuned by adjusting the polarity of IPA:EtOH mixtures. FT-IR indicated that this was indeed the case (Figure 1b). We further observed that the optical transparency qualitatively increased with decreasing solvent polarity (Figure 1c). Notably the absorption was decreased across the visible spectrum and into the UV range, with minimal absorption for all wavelengths ≥250nm, (Figure S2).

This was confirmed quantitatively, as we found that both DS_{rel} and transparency increased gradually with decreasing polarity of the solvent mix from 1:2 IPA:EtOH to pure IPA (Figure 1d). This trend was further confirmed when determining the degree of substitution via titration (Figure 1e). Interestingly, when we repeated the solvent composition study with lower amounts of reactants 1.25:1 NaOH:AGU and 0.5:1 MCA:AGU, the degree of control was somewhat diminished. For this set of reactants, the DS_{rel} as well as the transmittance, was negligible for all solvent mixtures except pure IPA (Figure S3). Also, for this condition we observed a large variance in the degree of reaction. We speculate that this could be due to a larger sensitivity to external factors that were not controlled such as the humidity. We thus conclude that the degree of substitution can be fine-tuned by changing the polarity of IPA:EtOH mixed solvents for reactant concentration of at least 2.5:1 NaOH:AGU and 1:1 MCA:AGU. The degree of substitution further

correlated with transparency, yielding highly transparent fibers for IPA:EtOH solvent mixtures containing at least 66% v/v IPA.

The increasing transparency of the fibers indicates a decrease in fiber size as well as a better dispersion of the fibers. To evaluate fiber size as a function of IPA:EtOH solvent composition, we applied electron microscopy, see Figure 2. Interestingly, SEM analysis showed that the average fiber diameter gradually decreased from roughly 350 nm to 250 nm when increasing the IPA content, while maintaining lengths of tens of microns or more across all conditions. These observations were in excellent correlation with transparency data. Moreover, the SEM data showed that we successfully achieved transparent fiber samples that maintained physiologically relevant sizes. Still, while micrometer-long fibers dominated, smaller structures could also be identified in TEM, especially for the reactions in pure IPA (Figure S4). Thus, for the majority of our subsequent studies we focused on the transparent nanofiber samples obtained when performing the carboxymethylation in 2:1 IPA:EtOH. Given their dimensions, we will refer to the modified cellulose fibers as carboxymethylated nanofibrillar cellulose (cNFC) in the remainder of the manuscript.

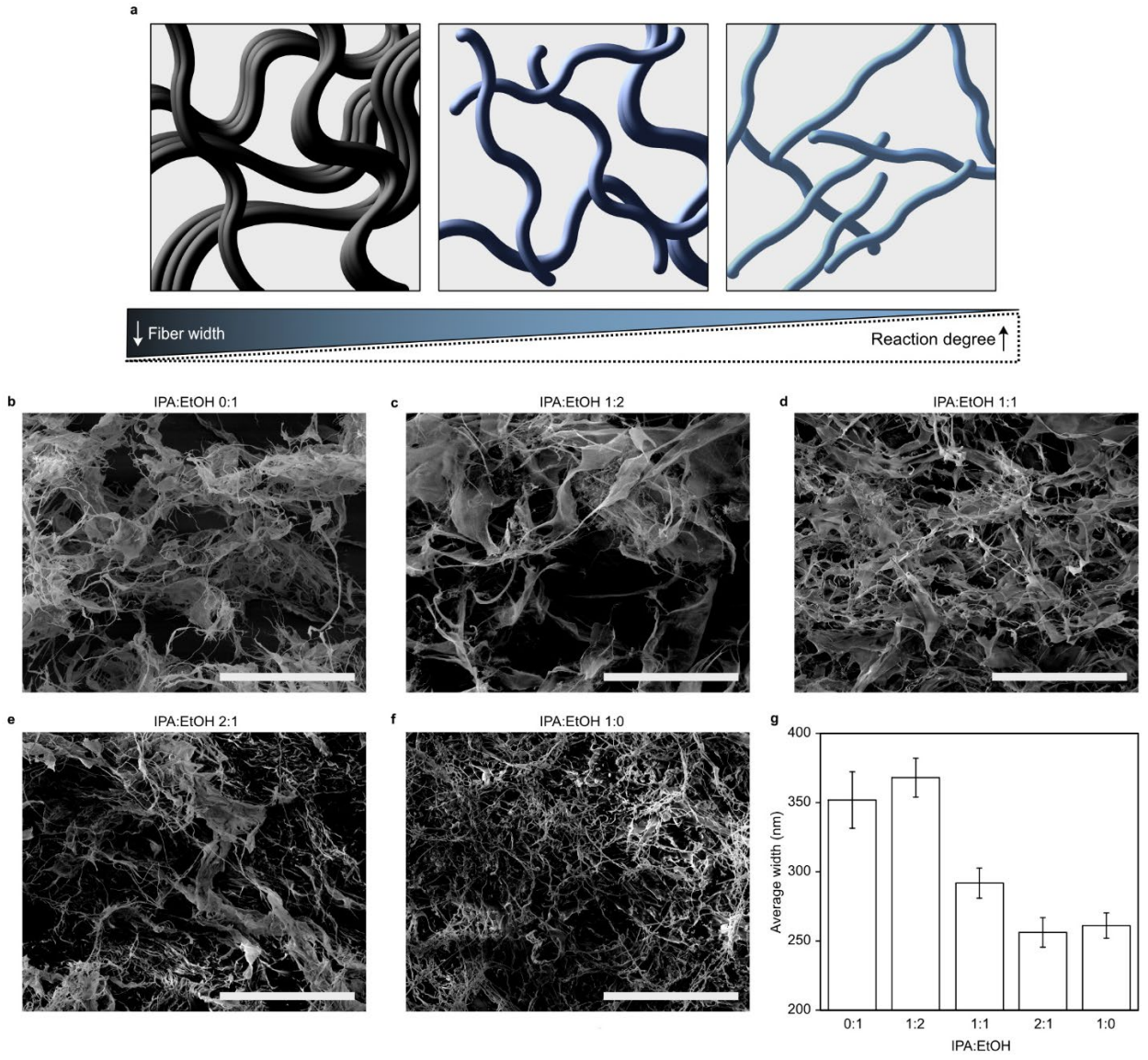

Figure 2. Size and appearance of carboxymethylated fibers analyzed via SEM. (a) Illustration of breakdown of fibers with increasing degree of reaction. (b) SEM images of fibers reacted in 0:1, (c) 1:2, (d) 1:1, (e) 2:1, and (f) 1:0 IPA:EtOH. Scale Bar: 50 µm. (g) Average fiber width in nm and SEM for n = 100, calculation based on different fields of view of same sample.

While all the carboxymethylated cellulose fibers preserved lengths of at least tens of micrometers, the rheological properties were affected notably with increasing degree of

substitution, see Figure 3a-f. For samples with a low degree of substitution, shear-thinning gels with a defined yield stress were maintained for 1% w/v samples. However, for transparent samples with a higher degree of reaction, these beneficial properties for 3D printing were largely lost (Figure 3g). However, the rheological properties required for 3D printing can be recovered by adjusting fiber concentration. (Figure 4a-c). Specifically, by increasing the concentration up to 3% w/v the transparent fibers obtained by carboxymethylation in 2:1 IPA:EtOH, shear thinning gels were re-established. As expected, these rheological improvements are immediately reflected in excellent 3D printing properties (Figure 4d-f). Moreover, the storage modulus of the shear-thinning gels could be tuned in the printable window from ~50 Pa to ~2.5 kPa, by increasing cNFC concentration, thus spanning a large part of the physiologically relevant range for soft tissue, (Figure 4g). Importantly, increasing the fiber concentration only lead to minor decreases in sample transparency and the transmittance did not fall below 95% in a 3% w/v fiber solution, (Figure 4h). Therefore, it is possible to recover printability and shape fidelity of the fiber dispersion by increasing its concentration, without losing transparency.

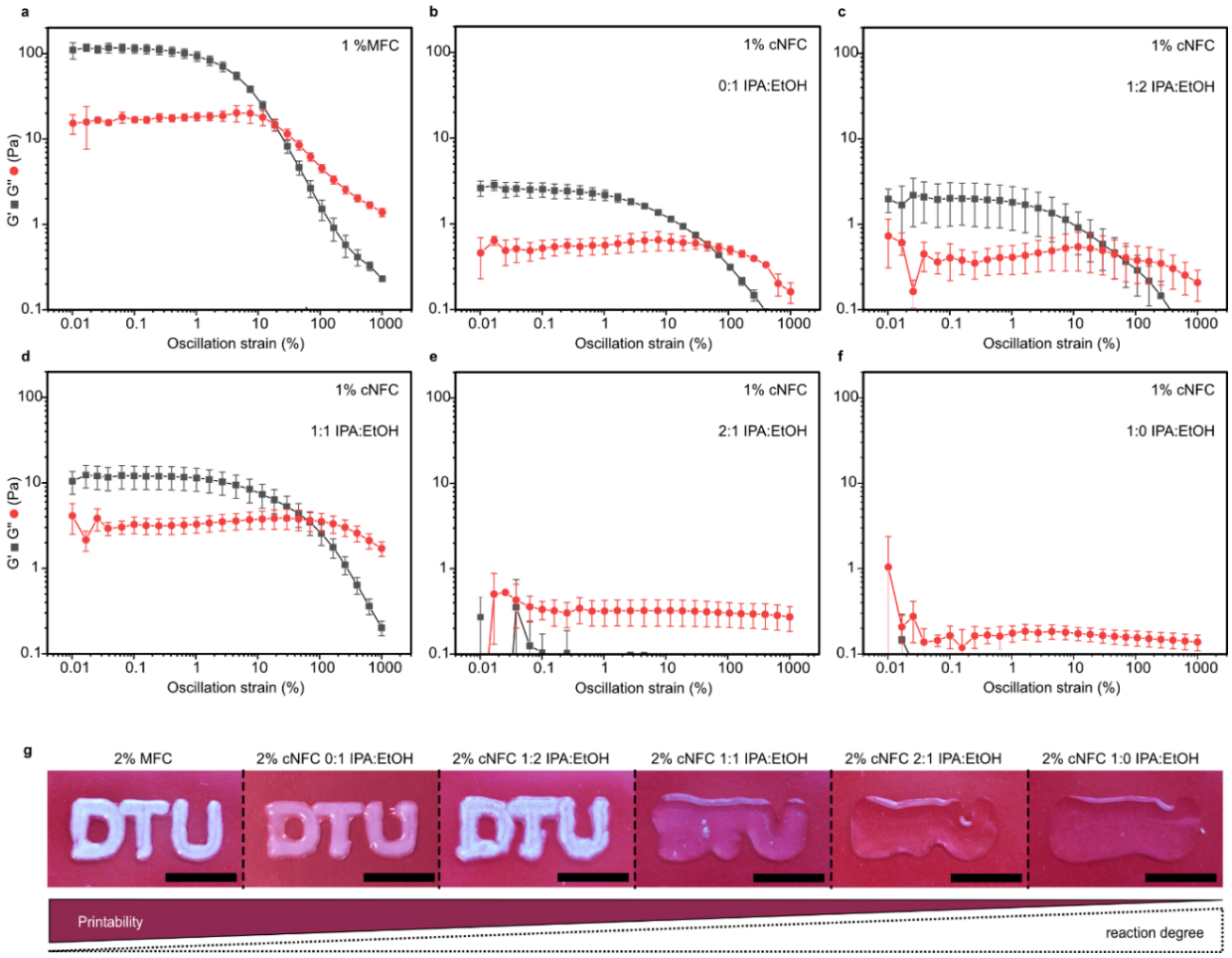

Figure 3. Rheology and printability of carboxymethylated fibers at 1% in milliQ water. Storage modulus G' and Loss modulus G'' of (a) MFC, fibers oxidized in (b) 0:1, (c) 1:2, (d) 1:1, (e) 2:1, and (f) 1:0 IPA:EtOH. Determined in oscillation sweep recorded at 25°C in milliQ water at 1 Hz. SEM for n = 3. (g) Optical appearance and print of DTU logo with steel needle (ID 400 µm) with 2% MFC, 2% cNFC 0:1, 2% cNFC 1:2, 2% cNFC 1:1, 2% cNFC 2:1, and 2% cNFC 1:0. Scale bars = 1 cm.

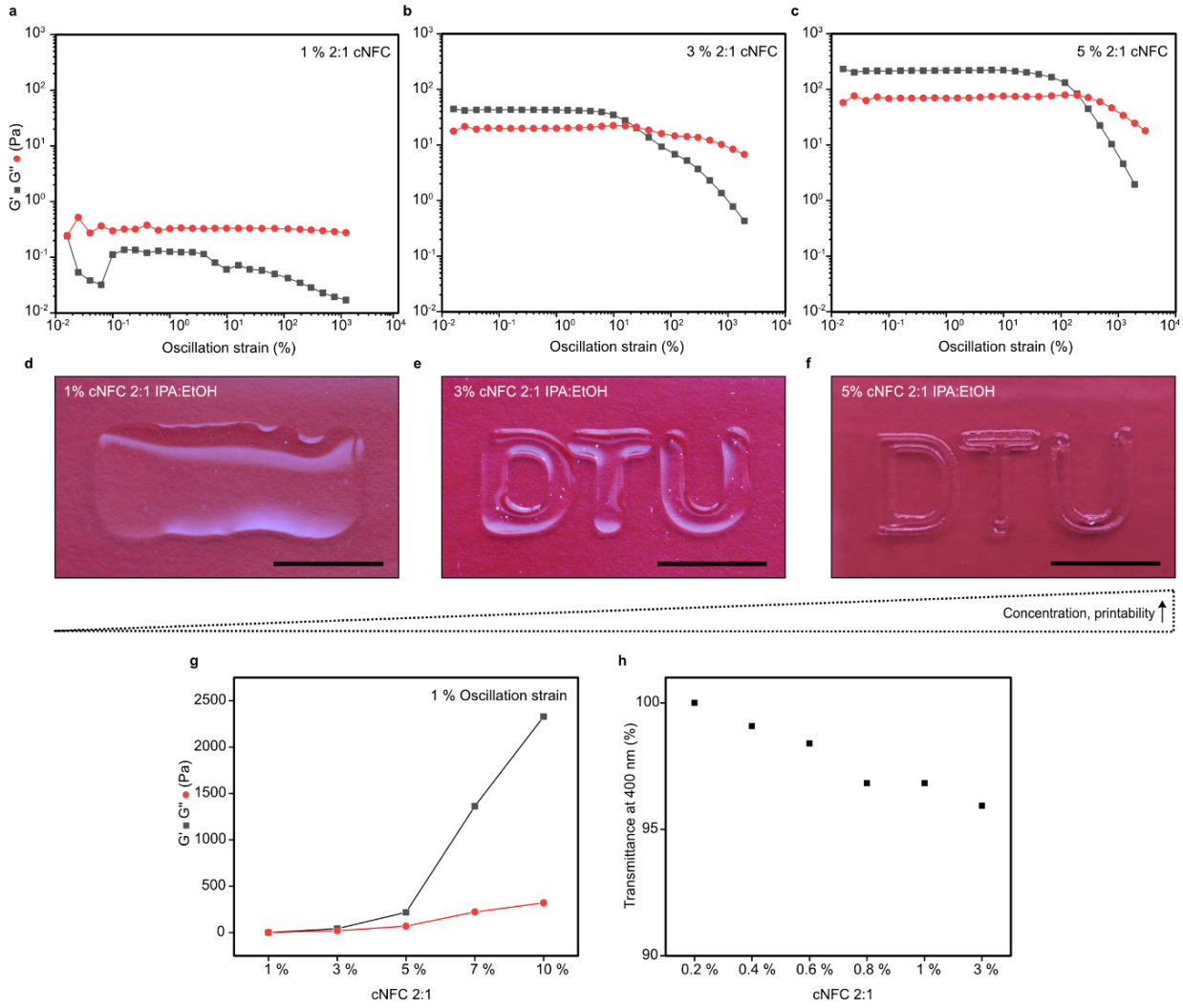

Figure 4. Rheology, transmittance and printability of cNFC 2:1 at higher concentrations. Storage modulus G' and Loss modulus G'' of (a) 1 % cNFC 2:1, (b) 3 % cNFC 2:1, and (c) 5% cNFC 2:1. The oscillation sweeps were recorded at 25°C in milliQ water at 1 Hz. (d) Printability of DTU logo at 1 %, (e) 3%, and (f) 5% cNFC 2:1 in milliQ water. Scale bar = 1 cm. (g) Storage G' and loss G'' modulus at 1 % oscillation strain as a function of increasing concentration of cNFC 2:1 in %. (h) Transmittance at 400 nm in (%) as a function of increasing concentration of cNFC 2:1 in milliQ water.

The excellent shape fidelity at higher cNFC concentrations allowed us to develop cross-linkable inks for complex structures. As example, we formulated composite inks composed of cNFC and alginate. Notably, MFC:alginate inks have been studied extensively for bioprinting, yet for unreacted fibers these composites have very limited transparency[7]. To generate an optically transparent alternative, we formulated a cNFC:alginate ink with similar rheology to MFC:alginate. This required using slightly higher concentration of cNFC than MFC (Figure 5a-c). The shape fidelity and transparency of an example octopus figurine was intact throughout printing and crosslinking for cNFC:alginate (Figure 5d).

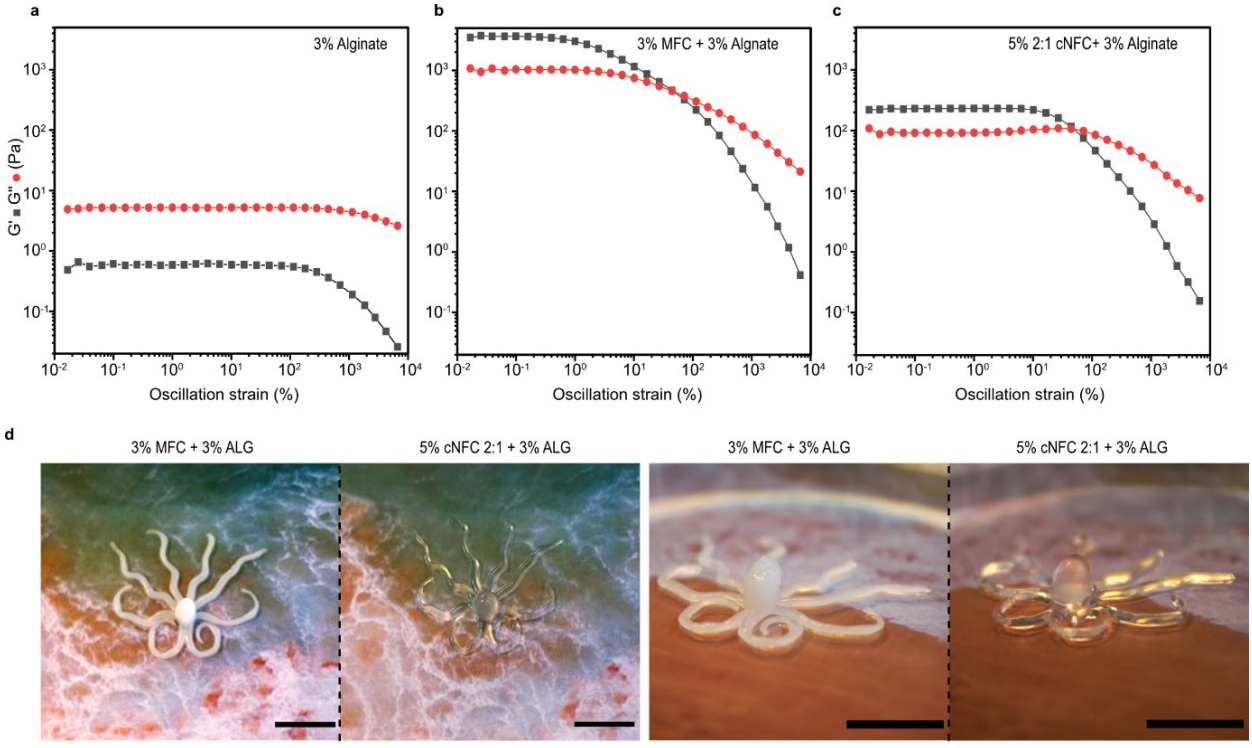

Figure 5. Rheology and 3D print of cross-linkable cNFC:alginate composite inks. Storage modulus G' and Loss modulus G'' for (a) 3% alginate. (b) 3% MFC + 3% alginate composite ink. (c) 5% cNFC 2:1 + 3% alginate composite ink. The oscillation sweeps were recorded at 25°C in

milliQ water at 1 Hz. (d) Side by side comparison of Octopus figurine printed with 3% MFC + 3% alginate and 5% cNFC 2:1 + 3% alginate composite inks. (Scale bars = 1 cm).

Although alginate is a widely applied biomaterial, cNFC:alginate is largely irrelevant as ECM-mimicking bioink since it lacks the native protein landscape and cell-adhesive motifs. As a simple solution, we found that the cNFC was readily miscible with both gelatin and collagen-based gels at a wide range of ratios and concentrations. Notably, this is not the case for unmodified MFC, where phase separation occurs. For formulating cNFC:gelatin inks, we aimed to decouple ink gelation and rheology during printing from stiffness of the final printed construct (Figure 6, Figure S6). This would be advantageous as compared to pure gelatin or gelatin-methacrylate inks, where these properties are highly correlated and thermal control during printing is essential. For our composite inks, we thus focused on low Bloom gelatin at low concentrations that do not gel at RT (Figure 6a). On the other hand, since cNFC behaves like physical gels with concentration-defined yield stress for concentrations ≥3% w/v, the rheology of cNFC:gelatin inks at RT can be completely dominated by the fiber content at RT (Figure 6b-c, Figure S6). Yet, while cNFC content dominates printability, gelatin content largely defines the final stiffness of the final material after cross-linking enzymatic microbial transglutaminase (mTG) (Figure 6d-e, Figure S6). It is thus straight-forward to formulate printable cNFC:gelatin composite inks with independent control of flow and final material mechanics (Figure S6). We found the Young's modulus of cNFC:gelatin matched well with that of native muscle tissue[39] when combining ~5% w/v cNFC and ~5% w/v gelatin (Figure 6e).

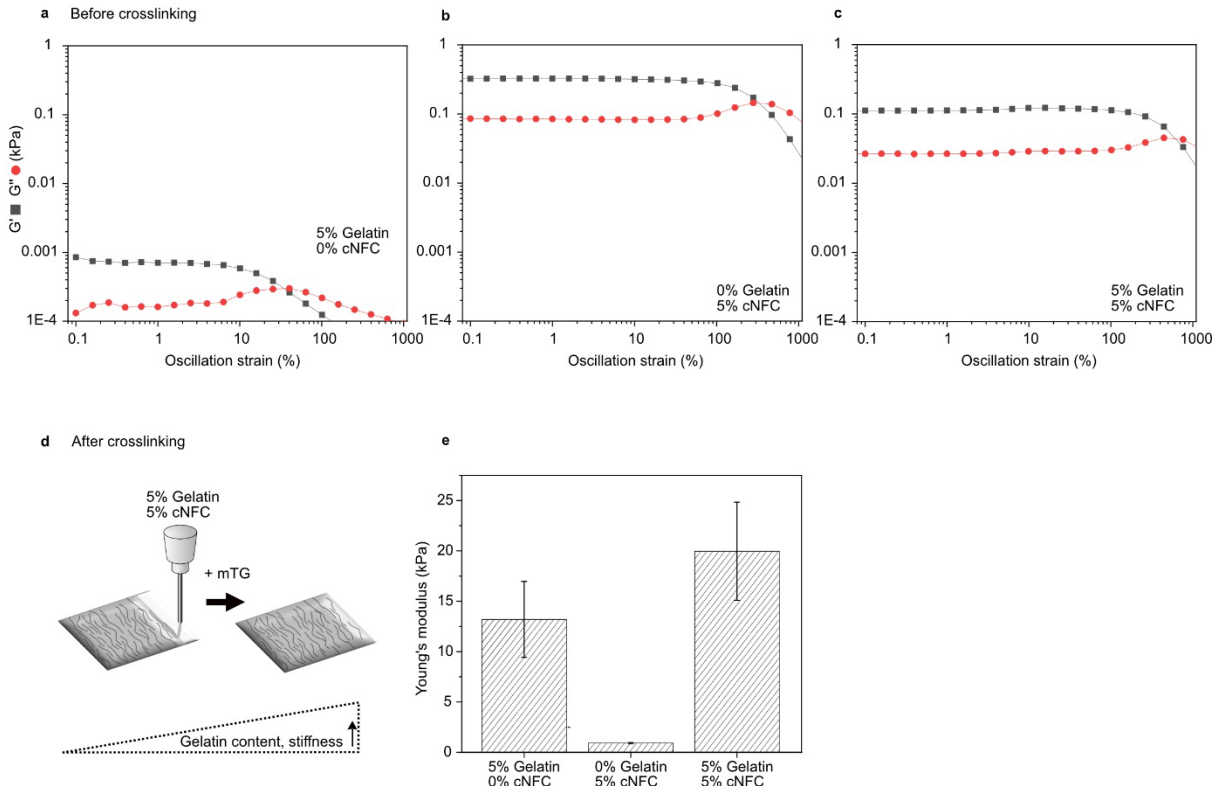

Figure 6. Rheology and stiffness of cNFC:gelatin composite inks before and after crosslinking. The oscillation sweeps were recorded at 25°C in Dulbecco's modified eagle's medium (DMEM) at 1 Hz. Rheology of (a) 5% gelatin + 5% cNFC, (b) 0% gelatin + 5% cNFC and (c) 5% gelatin + 0% cNFC composite inks. (d) Illustration of printing of cell-instructive coatings: substrates are subsequently cross-linked with mTG at 4 °C overnight. (e) Young's modulus E in kPa of cross-linked substrates printed with 5% gelatin + 5% cNFC, 5% gelatin + 0% cNFC, and 0% gelatin + 5% cNFC composite inks. E calculated from G' at 1 % oscillation strain and SEM for n=3.

Given their structural similarity to native collagen, we hypothesized that the cNFC fibers may serve as cell-guiding structures within cNFC:gelatin composites. Further, inspired by previous studies that have used extrusion-driven orientation of cellulose fibrils during 3D printing as basis for composites with programmable swelling or diffraction[18,19], we aimed to explore if of cNFCs would suffice to define the orientation of cells and tissues. To test this hypothesis, we printed a range of planar cNFC:gelatin tissue culture substrates, and studied whether murine C2C12 myoblasts developed into myotubes that followed the print direction. At a constant gelatin concentration of 4% w/v, we observed a gradual improvement in orientation of myotubes with increasing fiber concentration and highly parallel alignment for cNFC concentrations ≥ 4% w/v (Figure S7), and at 5% w/v gelatin with 5% w/v cNFC (Figure 7a-d, Figure S8). Notably, macroscopic surface from filaments was negligible (Figure S9), and cellular orientation was thus in all likelihood caused by shear induced orientation of fibers (Figure S10). This print-guided orientation was highly controllable, as we could easily generate complex circular and checkerboard geometries (Figure 7e, f).

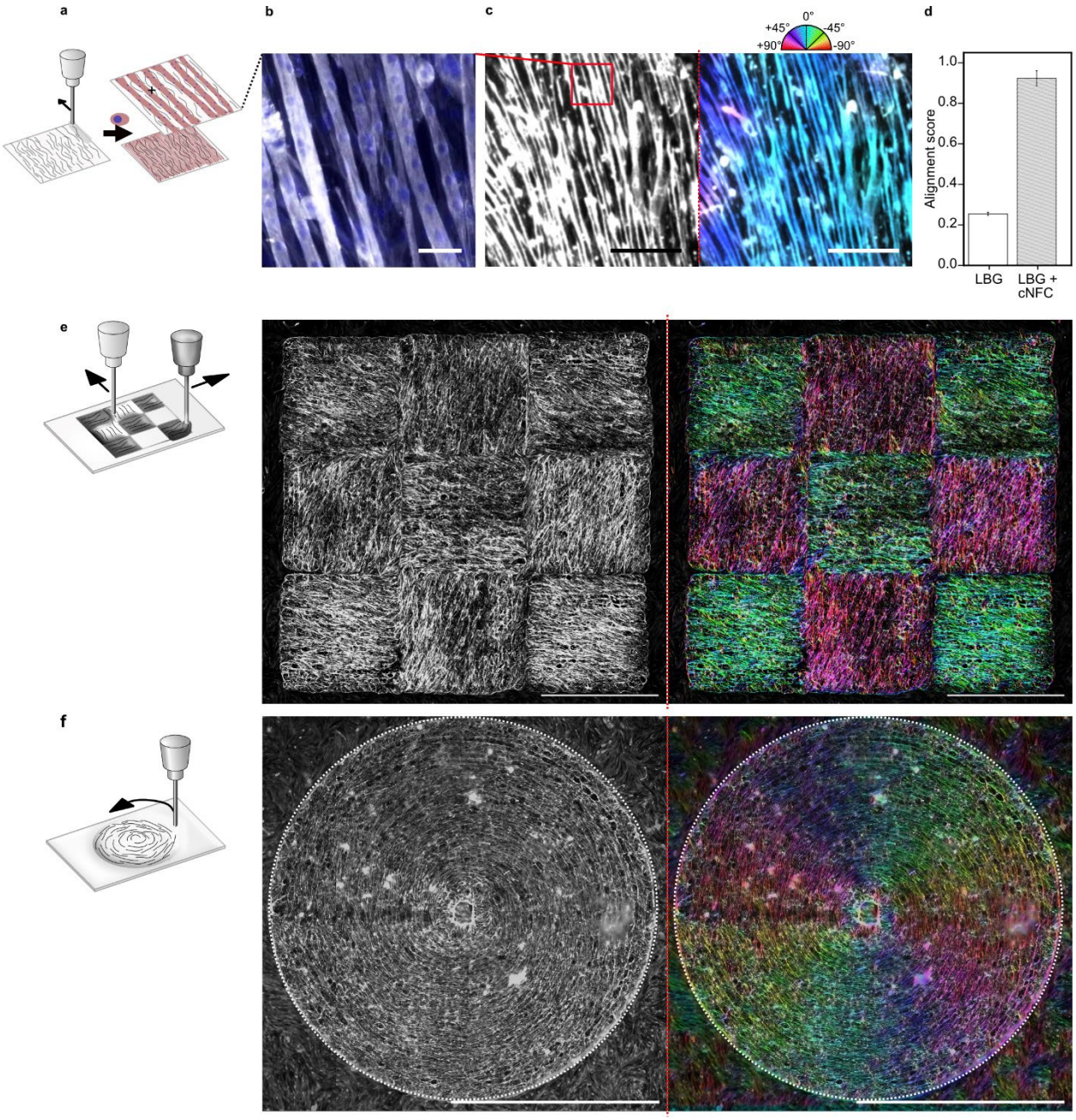

Figure 7. Self-alignment of C2C12 on cNFC:gelatin substrates. (a) Illustration of seeding of C2C12 muscle cells onto cross-linked, printed substrates. (b) Polynucleated myotubes of seeded cells differentiated on printed substrate. White: Actin. Blue: Nucleus. Scale bar: 50 µm. (c) False-color mapping of myotube (actin) orientation with OrientationJ. Scale bar: 500 µm. (d) Alignment score (0-1) of C2C12 myotube alignment on 5% LBG compared to 5% LBG + 5% cNFC. SEM

for n = 3. (e) Illustration of printing of alternating blocks of horizontal and vertical lines in a checkerboard-like fashion and false-coloured 15x15 mm checkerboard with alternating orientation of seeded cells. Scale bar: 5 mm. (f) Illustration of printing of concentric circles with r = 3.5 mm and false-coloured print with circular oriented cells. Scale bar: 5 mm.

Beyond C2C12 cells, the substrates were also well-suited for orienting of human skeletal myotubes derived from primary myoblasts (Figure 8). These substrates enabled extended myotube culture and maturation, as we observed no indication of cytotoxicity or myotube delamination during 17 days of maturation of the human samples (Figure S11). Moreover, we observed an improvement in myotube thickness during extended culture and physiological responses to insulin stimulation, indicative of native-like metabolic functionality (Figure S11). Beyond programmable soft tissue culture substrates, cNFC:gelatin could also be formulated into bioinks with embedded myoblasts for room-temperature bioprinting. Here, our preliminary studies indicated that a high fiber content could limit cell spreading and division. We therefore applied a lower cNFC content of 2% w/v and 4% w/v gelatin in the inks. During culture, these bioprinted myoblasts developed into polynucleated myotubes (Figure S12).

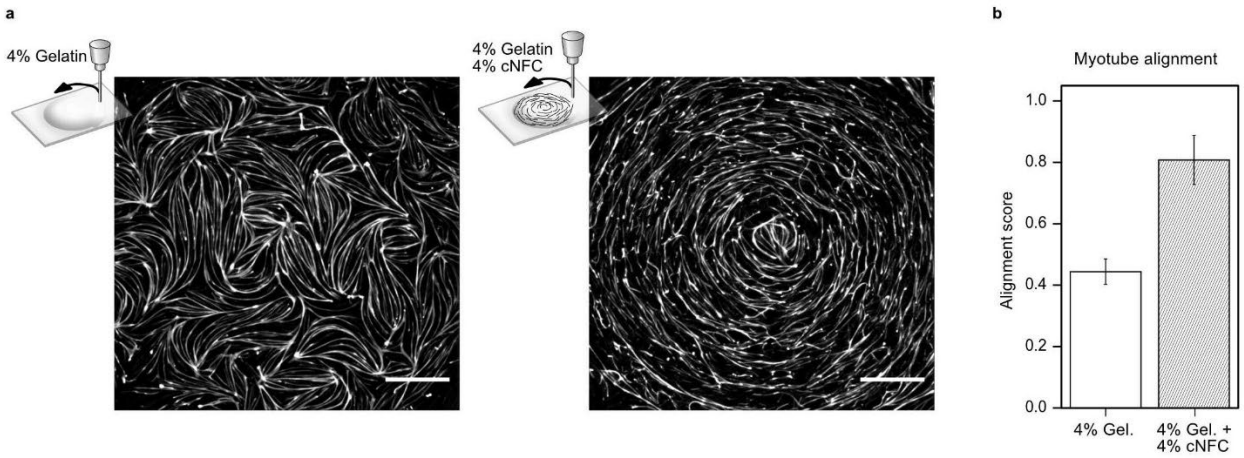

Figure 8. Self-alignment of human skeletal myocytes (HSkM) on printed cNFC:gelatin substrates. (a) Alignment of HSkM according to print direction. Substrates were printed with a steel nozzle (ID 250 µm) in circular motion with 4% gelatin (left) and 4% LB gelatin + 4% cNFC (right). White: Actin-stain. Scale bar: 1.5 mm. (b) Alignment score (0-1) of human myotubes aligned on 4% LB gelatin and 4% LB gelatin + 4% cNFC. SEM for n = 3.

DISCUSSION

Cellulose nanofibers are appealing for extrusion-based 3D printing and biomedical applications due to their accessibility, biocompatibility, and shear-thinning properties. However, such fibers may have radically different properties and size dependent on their preparation. Thus far micron-scale opaque MFC or tiny nano-crystalline fibers have received considerable attention[7–11,21,22], as these can be generated with relative ease[24,30]. We hypothesized that intermediate sizes that mimic the size of native collagen fibers, may have unique properties for tissue engineering applications. To generate such fibers, we established a procedure for tuning the carboxymethylation of MFC to yield transparent, ten-to-hundreds of µm long cNFC. In the process, we observed that the

carboxymethylation reaction can be closely controlled by adjusting the composition of IPA:EtOH solvent mixes. This is likely caused by the low solubility of NaOH in IPA: When NaOH is added to the dispersed fibers, the driving force to accumulate on the surface of the hydrated fibers is higher with increasing IPA content[29]. The activation of the alcohol-groups by NaOH is therefore highest in pure IPA, followed by 2:1 IPA:EtOH, which is reflected in the final DS. Following the reaction, we observed a decrease in viscoelasticity with increasing DS. However, SEM images indicated that long fibrils remained for all reaction conditions, which seems to exclude fiber breakdown as the reason for the decrease in mechanical properties. Instead, we propose that accumulation of surface charge as well as recrystallization of the cellulose are likely explanations. Indeed, organic solvents can induce decrystallization and changes in the polymorphism of cellulose, which can notably decrease cellulose stiffness[40,41]. Still, we were able to restore the shear-thinning properties and shape-fidelity by increasing the concentration of fibers in solution without a significant loss in transparency.

As cNFC fibers were readily dispersible and miscible with common hydrogel bio-materials, such as alginate, collagen, and gelatin, we were able to formulate a range of composite bioinks. Importantly, while cNFC provided excellent printability to such inks, the mechanical properties of e.g. cNFC:gelatin was dominated by gelatin after crosslinking. It is thus possible to decouple and independently control the mechanics during and after printing in these composite inks. Most importantly, we further found that cNFC provided unique anisotropic and cell-instructive properties to these common biomaterials. When differentiating human or mouse myoblast into myotubes on planar, 3D-printed cNFC:gelatin substrates, we observed a unidirectional alignment of myotubes along the toolpath applied in the printing. Notably, the degree of control was so high that we could easily organize myotubes into complex non-linear patters. Previously, similar shear-

induced alignment of cellulose fibrils has been applied as basis of 3D printed composites with programmable swelling or optical properties [18,19], however, to the best of our knowledge this effect has not been demonstrated as a method for organizing engineered tissues. We speculate that significant length of our transparent cNFC may be critically important in this regard. Notably, the fiber length significantly exceeds that of a single myoblast, meaning that each fiber may serve as physical cue for several myoblasts prior to their fusion into myotubes.

Soft and structured hydrogel substrates have previously been shown beneficial for self-organization, long-term culturing and maturation of engineered striated muscle tissues[32–34,42]. Similarly, synthetic nanofiber scaffolds produced e.g. by force-spinning or electrospinning, are efficient for generating anisotropic engineered muscle tissues[35,36,43]. More recently, printed composites composed cellulose fibrils and hyaluronic acid methacrylate, have also been explored from organizing fibroblasts[44].Similarly previous anisotropic soft substrates for muscle, printed cNFC:gelatin enable maturation of humans myotubes for at least several weeks. The myotubes displayed steadily increase in size and basic metabolic function, indicating that cNFC:gelatin composites were not cytotoxic. This is in good agreement with earlier reports studying where CNF and CNCs were found not to be cytotoxic[45]. Further, we speculate that the extensive length of the present cNFCs, will lower the risks of cellular uptake or lysosomal damage. Indeed such risks have been reported to occur mainly for tiny CNCs with lengths in the order of hundreds of nanometers[45]. It is worth stressing that we have not considered or studied the use of cNFC for in vivo uses where e.g. foreign body reaction could be a concern.

However, we believe that 3D printing of cNFC:gelatin carries unique practical advantages for in vitro tissue modelling, as the procedure can readily be customized and adapted to a range of culturing formats, not least multi-well plates. Moreover, since it does not rely on high-resolution

nozzles and is inherently a single step procedure conducted a RT, it is highly scalable. Given the thixotropic and tissue-guiding properties of the cNFC, an additional and potentially larger impact may lie within their application in 3D bioprinting of cell laden inks. Within this paper, we showcased this application in proof of principle printing of 3D muscle strips, where we again combined cNFC with gelatin to achieve cross-linkable bioinks. In these studies, we observed that cell-spreading and division appeared to be diminished for when applying high cNFC concentrations. We propose that this was mainly caused by the lack of cell-adhesive motifs on the cNFCs. It is however worth noting that for high fiber concentrations the risk of damaging embedded cells is also increased, as the high viscosity will produce a higher shear-stress on the cells upon extrusion[46]. We therefore applied only 2% w/v in these inks. Given the low fiber concentration, the myotubes elongation and alignment was in this case largely a product of filament geometry. Therefore, for broadening our approach and tailoring cNFC-based bioinks more closely to a given tissue, an important future direction will be the functionalization of carboxylic groups of cNFC with tissue-specific and cell adhesive proteins and peptides. This may ultimately enable more specific inks and cross-linkable inks based solely on cNFCs.

CONCLUSION

In this study, we detailed a robust procedure for generating transparent, dispersible and cell-instructive cellulose nanofibrils and 3D printing bioinks. A key foundation for the procedure is the observation that the degree of carboxymethylation can be accurately controlled by adjusting polarity of ethanol-isopropanol reaction solvents. In doing so, we generated transparent cellulose fibers with excellent 3D printing properties that mimic the size and shape of native ECM protein fibers. When applying these cellulose nanofibers in composite bioinks, we were able to predict

and control the tissue-level organization of human and murine skeletal myotubes by extrusion direction and pattern. The aligned and extended myotubes could be matured for several weeks, making our approach relevant as a scalable method for generating physiologically relevant models of human muscle. The functional groups introduced through the carboxymethylation further provides means of tailoring of nanofiber biochemistry, which significantly broadens their future relevance for tissue-engineering applications.

MATERIALS AND METHODS

Carboxymethylation

MFC was obtained from Norwegian spruce by Borregaard in Sarpsborg (NO) and delivered as 10% aqueous paste. Isopropanol (IPA), methanol and ethanol absolut ≥ 99.9% were purchased from VWR and always freshly opened before each experiment as the usage of old IPA and EtOH will reduce the reactivity of the reactants. NaOH (S5881) and monochloroacetic acid (MCA, 402923) were purchased at Sigma Aldrich as solids. First, MFC was disintegrated using an Ultra-Turrax homogenizer with a S25N - 18G - ST dispersing element. The dispersion was conducted in pure solvent and the following solvent combinations IPA:EtOH: 0:1, 1:2, 1:1, 2:1, 1:0. . The day before the experiment, a 5% w/v NaOH (2% w/v in pure IPA) solution was prepared in the respective solvent. The day after, 10 g of MFC pulp (1 g dry content) were homogenized for 10 min. at 10,000 rpm. The homogenized MFC was heated up to 35 °C while stirring. 12 mL of a 5% w/v NaOH solution (600 mg) were added to the dispersed fibers and left stirring at 35 °C for 30 min. After, the temperature was increased to 45 °C. Once the temperature was reached, 4 mL of a 142.2 mg/mL (570 mg total) MCA solution in the respective solvent was added and left stirring at

45 °C for 3 h. The substitution reaction was repeated in the same solvents with half amount of reactants (300 mg NaOH and 285 mg MCA).

Around 10 mL of a 10% v/v acetic acid solution was added to the fibers for neutralization and the fibers were filtered. The filtered fibers were washed 3x with methanol, followed by dialysis against deionized water for three days in a 12-14 kDa cut-off dialysis tube with 2 daily water changes. The dialyzed fibers were freeze-dried and stored at room temperature until further use.

IR

IR spectra were recorded on a PerkinElmer Spectrum 100 FT-IR spectrometer. The spectra were recorded with a resolution of 1 cm^{-1} from 4000 – 800 cm^{-1}. All spectra were recorded in absorbance units and normalized at 1050 cm^{-1}. The relative degree of substitution (DS_{rel}) was calculated by relating the intensity of the normalized absorbance (NA) of the stretching vibration of the carboxyl group (C=O) at 1595 cm^{-1} to the stretching vibration of the glucose backbone (C-H) at 2894 cm^{-1}:

$$[1] \qquad DS_{rel} = \frac{NA_{1595\ cm^{-1}}}{NA_{2894\ cm^{-1}}} - C$$

The constant C indicates the relation between these two stretching vibrations of the carboxyl group and glucose backbone in non-oxidized cellulose.

Titration

Between 20 and 50 mg of cNFC were weight in and transferred to a clean 100 mL Erlenmeyer flask. Calcium acetate (10229177, Thermo Fisher) solution 2 % w/v was added to the fibers (10 ml) and let the solid material imbibe for 30 minutes. 2 drops of phenolphthalein indicator

(A0424229, Thermo Fisher) were added to the flask (prepared as 1.0 % w/v in ethanol). A burette was filled with standardized NaOH solution (0.0121 M or 0.00121 M). The cNFC solution was titrated until the faint, pink endpoint is reached (persisting for at least 30 seconds). Three separate weighed samples of each cNFC sample were analyzed. The percentage of carboxyl content was calculated using the following equation:

$$[2] \qquad \text{Carboxyl groups } [\%] = \frac{\mathrm{N \cdot V \cdot MW_{COOH}}}{\mathrm{m[mg] \cdot 100}}$$

Where N is normality of NaOH solution, V is the volume of NaOH consumed to reach the endpoint (corrected for the blank). MWCOOH is 59, corresponding to the introduced group -CH2COOH.

Transmittance

The absorbance of MFC and cNFC was measured using a Thermo Scientific NanoDrop 2000, at a path length of 1 mm. In general, the samples were homogenized at 1 % w/v for 10 min. using an Ultra-Turrax homogenizer at 10,000 rpm for 10 min. The absorbance was measured immediately after homogenization.

Rheology

The rheology of each ink was analyzed using a Discovery Hybrid Rheometer (TA instruments, DE, USA) equipped with a Peltier plate thermal controller and a plate geometry with a diameter of 40 mm and a fixed gap of 1 mm. All samples were freshly prepared right before measurement. Fiber dispersion where prepared right before measurement and homogenized as described before. As a standard, amplitude sweeps were recorded at 25°C in milliQ water at 1 Hz at an oscillation

strain of 0.01 – 10,000 %. For calculation of Young's modulus, hydrogel precursor solutions with desired conditions (gelatin and cNFC content) were casted in between two poly(methyl methacrylate) (PMMA) slides with 1 mm spacer. Prior to gelation, the slides were coated with polyvinylalcohol to avoid the hydrogel from sticking to the PMMA surfaces. The hydrogels are incubated at 4 °C for 30 min. to achieve pre-polymerization of gelatin. Then, the PMMA slides were removed and the gels are replaced in the micro plate with 10 U/ml mTG solution for 1 day at 4 °C to achieve the enzymatic cross-linking. The storage modulus of the gels was determined by performing oscillatory shear experiments with parallel plate geometry as described above. The Young's modulus E is calculated as follows $E=2G'(1+\nu)$, assuming $\nu = 0.5$.

SEM

Freeze-dried fibers were deposited on a carbon sticker. The samples were sputtered with a 2.4 nm gold layer. Images were recorded using a Quanta 200 FEG Cryo ESEM at an acceleration voltage of 5 kV, an aperture of 40 µm, spot size of 3.5 µm and working distance of 6 mm. Different fields of view of the same sample were analyzed at different magnifications and used for fiber counting.

TEM

5 µl of fiber solution was drop cast onto freshly glow discharged carbon stabilized formvar coated 200 mesh nickel TEM grids (EMS Diasum). The fibers were allowed to adsorb for 5 min. before the excess solution was wicked away using filter paper. The fibers were imaged using a Tecnai T20 G2 TEM at 200 kV and images were acquired using a TVIPS XF416 CCD camera.

Printing of 3D figurine

A 3D computer aided design (CAD) of an octopus was created using Fusion360 and printed on a RegenHU 3D Discovery bioprinter. A cross-linkable composite-ink based on non-reacted MFC was prepared using 3% w/w MFC and 3% w/v alginate (Dynamic viscosity: 80-120 cP, 194-13325, FUJIFILM Wako) in milliQ water. The MFC:alginate composite-ink was printed with a pneumatic syringe and a steel nozzle (ID 250 µm, Cellink Swe) at a pressure of ~ 230 kPa. A transparent, cross-linkable composite-ink was prepared using 5% w/v cNFC and 3% w/v alginate in milliQ water and printed with a pneumatic syringe and steel nozzle (ID 250 µm, Cellink Swe) at ~ 560 kPa.

Culturing of C2C12 murine myoblasts

C2C12 cell-culture was performed under sterile conditions and incubated at 37 °C, 100% humidity, 5% CO_2. C2C12 murine myoblasts were cultured in growth medium containing DMEM (D5796, Sigma-Aldrich), 10% fetal bovine serum (S1810, Sigma-Aldrich) and 1% P/S (P0718, Sigma-Aldrich). Cells were passaged and harvested at 80% confluency. All cells were kept within 10 passages from stock. Differentiation was initiated by changing growth medium to differentiation medium containing DMEM, 2% horse serum (H1270, Sigma-Aldrich).

Culturing of human primary skeletal muscle cells

Human single-donor skeletal muscle cells (SK111, Cook Myocite) were maintained and passaged in myotonic basal media (MB-2222, Cook Myocite) supplemented with 10% myotonic growth supplement (MS-3333, Cook Myocite) and 1% P/S antibiotic in a humidified atmosphere containing 5% CO_2 and 95% air at 37°C.

Printing of cell-instructive surface and cell seeding

The following procedure was performed under sterile conditions: sterile solvents with 1% penicillin/streptomycin (P/S, P0718, Sigma-Aldrich) were used and cross-linking solutions were sterile filtered with a 0.45 µm pore sized filter. All syringes and needles were additionally sterilized with UV light. A composite ink consisting of 5% w/v low bloom gelatin (164 G bloom, 48723, Sigma Aldrich) and 5% w/v cNFC was prepared as follows: dried fibers were suspended in DMEM at 10,000 rpm for 10 minutes. Low bloom gelatin was added to the fiber suspension and heated to 45 °C for approx. 45 minutes. The solution was stirred from time to time with a spatula and shortly centrifuged to exclude air bubbles. The composite ink was printed with a steel nozzle (ID 200 µm, Cellink Swe) at a pressure of 580 kPa and feed rate of 12 mm/s. Subsequently, the print was cross-linked with a 5 U/mL microbial transglutaminase (mTG, ACTIVA® TI Transglutaminase, 100 U g^{-1}, 1002, Modernist Pantry) solution over night at 4 °C. Before cell-seeding, the prints were washed 3x for 10 min. with PBS (D8537, Sigma-Aldrich). Alignment experiment in Figure 7 was performed with murine C2C12 myocytes at a density of 20,000 cells per well of a 12-well plate. Differentiation was initiated after day 3 by changing the medium from growth medium to differentiation medium. The experiment was ended at differentiation day 7 by fixing the cells. Alignment experiment in Figure 8 was performed with human skeletal muscle cells at a density of 200,000 cells per well in 12-well plates directly on the printed substrates and kept in MEM (41090-028, Gibco) with 10% myotonic growth supplement for 2 days before differentiation were initiated by switching to 2% horse serum as growth supplement (26050088, Gibco). The samples in Figure 8 were fixed after 8 days of differentiation. The samples in Figure S11 were fixed after 10 and 17 days of differentiation.

Immunoblotting

Immunoblotting of S6 Ser235/236 and Akt Ser473 phosphorylation was performed by starving the myotubes from serum and glucose for 3 hours and then keeping them basal or stimulated with 1 or 100 nm insulin for 15 min prior to harvest. Samples were lysed in lysis buffer (50 mM Tris base, 150 mM NaCl, 1mM EDTA, 1 mM EGTA, 50 mM sodium fluoride, 5 mM pyrophosphate, 2 mM sodium orthovanadate, 1 mM dithiothreitol, 1 mM benzamidine, 0.5% protease inhibitor cocktail (P8340, Sigma Aldrich), 20% NP-40, pH 7.4. Western blot procedure was conducted as previously described[34]. The following antibodies from Cell Signaling Technology (US) were used: phospho (p)-Akt Ser473 (#9271), p-S6 Ser235/236 (#2211).

Bioprinting

A sacrificial ink was prepared consisting of 8% alginate (Dynamic viscosity: 300-400 cp, 192-09995, FUJIFILM Wako) and 10 U/mL mTG was prepared under sterile conditions. The sacrificial ink was printed at a feed rate of 15 mm/s with a pneumatic printhead at ~ 130 kPa with a plastic nozzle (ID 250 µm). A bioink consisting of 3% w/v cNFC and 6% w/v low bloom gelatin was prepared under sterile conditions. C2C12 skeletal muscle cells were harvested and mixed 1:4 with the bioink. The final concentrations were 2% cNFC, 4% low bloom gelatin, and 10 mio/mL C2C12. The print was performed at a feed rate of 15 mm/s with a pneumatic print head at approx. 25 kPa with a steel nozzle (ID 250 µm). Sacrificial and bioink were printed in parallel into a 12-well plate. The print was incubated at 4 °C for 5-10 min. to allow gelation of gelatin. Afterwards, a cold 10 U/mL mTG solution was added to each well and the print incubated at 37 °C for 1 h. The mTG solution was discarded and growth medium added to the wells. Differentiation was initiated at day 2. The samples were fixed at differentiation day 7.

Cell staining, fiber staining & imaging

Printed constructs were washed 3x with PBS. After, cells were permeabilized and fixed with 0.1% v/v Triton X and 4% v/v paraformaldehyde and incubated for 20 min. at RT. The prints were washed 3x with PBS while shaking. A 1:1000 dilution of 4′,6-diamidino-2-phenylindole, dihydrochloride (DAPI, 62247, Thermo Scientific), 1:200 dilution of Alexa Fluor™ Plus 555 Phalloidin (A30106, Thermo Fisher) for F-actin staining in PBS was added and incubated overnight at 4 °C. The prints were washed 3x with PBS and kept in PBS at 4 °C until further use. MFC was stained with calcofluor white (18909, VWR) by immersing the printed, dried substrate in 5mL of a 0.01% solution calcofluor white with 5 drops 10% KOH for 2 h. The substrate was rinsed and imaged with ProLong™ Gold Antifade (P10144, Molecular Probes). A 5% w/v cNFC ink was prepared by directly mixing 100 µL 0.01% calcofluor solution per 1 mL ink. The sample was printed and directly mounted with ProLong™ Gold Antifade. Images of fluorescent stains were recorded with a Nikon Eclipse Ti2 microscope and NIS-Elements software and a Zeiss Observer Z1 microscope with a mounted Zeiss AxioCam.

Myotube orientation quantification

The ImageJ plugin OrientationJ[47] was used to determine the orientation of the myotubes on printed substrates. For this, F-actin stain was recorded after 7 days of differentiation. The hue and saturation of the false colored images correspond to the orientation angle and coherency, respectively. The distribution of orientation was plotted against the principal orientation angle. The alignment score corresponds to the total fraction of distribution within ± 15 ° of the principal

orientation angle to the total count of oriented pixels. The alignment score was calculated for n = 3 fields of view of 1.75 mm x 1.65 mm of 3 different samples.

ASSOCIATED CONTENT

The following files are available free of charge:

Supporting information with additional data is included as a single PDF.

The supplementary information contains additional experimental data including, IR screening of carboxymethylation in different solvents; transmittance and absorbance spectra of cNFC reacted in IPA:EtOH mixtures; transmittance and Dsrel of carboxymethylation reaction with lower reactant content; TEM images; rheological studies; fiber-dependent alignment score analysis; brightfield image of fiber gel; stained fiber gels and cross-section of aligned cells on gel; human skeletal muscle cell myotube width analysis and immunoblotting; bioprint.example

Corresponding Author

Johan Ulrik Lind,

Department of Health Technology,

Technical University of Denmark,

Building 423 Room 012,

2800 Kgs. Lyngby,

DK - Denmark

Phone: +45 42 803 802

E-mail: joli@dtu.dk

Author Contributions

C.R.: designed and performed the experiments and composed the draft for the manuscript, R.P.: Assisted with experimental work and screening of reaction conditions, M.M. and S.B.: Performed rheology studies and chemical characterizations, J.R.K. and C-P.S.: Performed experiments with human cells, P.K.: Performed TEM analysis, T.L.A., C.K.P, T.E.J and J.U.L.: secured funding and designed study, J.U.L.: Supervised project and prepared manuscript. All authors revised and approved the final manuscript

ACKNOWLEDGMENT

C.R., R.P., S.B., M.M, J.U.L would like to gratefully acknowledge the Lundbeck Foundation (R250-2017-1425) and the Independent Research Fund Denmark (8048-00050 & 1032-00435)

for their support. J.R.K. acknowledges the generous support from the Danish Diabetes Academy (Novo Nordisk Foundation, NNF17SA0031406).

ABBREVIATIONS

3D, three-dimensional; AGU, anhydroglucose units; CNC, cellulose nanocrystals; cNFC, carboxymethylated nanofibrillated cellulose; ECM, extracellular matrix; ; EtOH, ethanol; dECM, decellularized ECM; IPA, isopropanol; MCA, monochloroacetic acid; MeOH, methanol; MFC, microfibrillated cellulose; mTG, microbial transglutaminase; NFC, nanofibrillated cellulose; PCL, polycaprolactone; PMMA, poly(methyl methacrylate); TEMPO, 2,2,6,6-tetramethylpyperidine-1-oxyl;

REFERENCES

(1) Lee, A.; Hudson, A. R.; Shiwarski, D. J.; Tashman, J. W.; Hinton, T. J.; Yerneni, S.; Bliley, J. M.; Campbell, P. G.; Feinberg, A. W. 3D Bioprinting of Collagen to Rebuild Components of the Human Heart. *Science* **2019**, *365* (6452), 482–487. https://doi.org/10.1126/science.aav9051.

(2) Skylar-Scott, M. A.; Huang, J. Y.; Lu, A.; Ng, A. H. M.; Duenki, T.; Liu, S.; Nam, L. L.; Damaraju, S.; Church, G. M.; Lewis, J. A. Orthogonally Induced Differentiation of Stem Cells for the Programmatic Patterning of Vascularized Organoids and Bioprinted Tissues. *Nat. Biomed. Eng. 2022 64* **2022**, *6* (4), 449–462. https://doi.org/10.1038/s41551-022-00856-8.

(3) Lind, J. U.; Busbee, T. A.; Valentine, A. D.; Pasqualini, F. S.; Yuan, H.; Yadid, M.; Park,

S. J.; Kotikian, A.; Nesmith, A. P.; Campbell, P. H.; Vlassak, J. J.; Lewis, J. A.; Parker, K. K. Instrumented Cardiac Microphysiological Devices via Multimaterial Three-Dimensional Printing. *Nat. Mater.* **2017**, *16* (3), 303–308. https://doi.org/10.1038/nmat4782.

(4) Sun, W.; Starly, B.; Daly, A. C.; Burdick, J. A.; Groll, J.; Skeldon, G.; Shu, W.; Sakai, Y.; Shinohara, M.; Nishikawa, M.; Jang, J.; Cho, D. W.; Nie, M.; Takeuchi, S.; Ostrovidov, S.; Khademhosseini, A.; Kamm, R. D.; Mironov, V.; Moroni, L.; Ozbolat, I. T. The Bioprinting Roadmap. *Biofabrication* **2020**, *12* (2). https://doi.org/10.1088/1758-5090/ab5158.

(5) Pless, C. J.; Radeke, C.; Cakal, S. D.; Kajtez, J.; Pasqualini, F. S.; Lind, J. U. Emerging Strategies in 3D Printed Tissue Models for in Vitro Biomedical Research. In *Bioprinting*; Conti, M., Marino, M., Eds.; Academic Press: Cambridge, US, 2022; pp 207–246. https://doi.org/10.1016/B978-0-323-85430-6.00007-8.

(6) Bowers, S. L. K.; Banerjee, I.; Baudino, T. A. The Extracellular Matrix: At the Center of It All. *J. Mol. Cell. Cardiol.* **2010**, *48* (3), 474–482. https://doi.org/10.1016/j.yjmcc.2009.08.024.

(7) Markstedt, K.; Mantas, A.; Tournier, I.; Martínez Ávila, H.; Hägg, D.; Gatenholm, P. 3D Bioprinting Human Chondrocytes with Nanocellulose–Alginate Bioink for Cartilage Tissue Engineering Applications. *Biomacromolecules* **2015**, *16* (5), 1489–1496. https://doi.org/10.1021/acs.biomac.5b00188.

(8) Kuzmenko, V.; Karabulut, E.; Pernevik, E.; Enoksson, P.; Gatenholm, P. Tailor-Made Conductive Inks from Cellulose Nanofibrils for 3D Printing of Neural Guidelines. *Carbohydr. Polym.* **2018**, *189*, 22–30. https://doi.org/10.1016/J.CARBPOL.2018.01.097.

(9) Im, S.; Choe, G.; Seok, J. M.; Yeo, S. J.; Lee, J. H.; Kim, W. D.; Lee, J. Y.; Park, S. A. An Osteogenic Bioink Composed of Alginate, Cellulose Nanofibrils, and Polydopamine Nanoparticles for 3D Bioprinting and Bone Tissue Engineering. *Int. J. Biol. Macromol.* **2022**, *205*, 520–529. https://doi.org/10.1016/J.IJBIOMAC.2022.02.012.

(10) Monfared, M.; Mawad, D.; Rnjak-Kovacina, J.; Stenzel, M. H. 3D Bioprinting of Dual-Crosslinked Nanocellulose Hydrogels for Tissue Engineering Applications. *J. Mater. Chem. B* **2021**, *9* (31), 6163–6175. https://doi.org/10.1039/D1TB00624J.

(11) Ojansivu, M.; Rashad, A.; Ahlinder, A.; Massera, J.; Mishra, A.; Syverud, K.; Finne-Wistrand, A.; Miettinen, S.; Mustafa, K. Wood-Based Nanocellulose and Bioactive Glass Modified Gelatin-Alginate Bioinks for 3D Bioprinting of Bone Cells. *Biofabrication* **2019**, *11* (3). https://doi.org/10.1088/1758-5090/AB0692.

(12) Kolesky, D. B.; Homan, K. A.; Skylar-Scott, M. A.; Lewis, J. A. Three-Dimensional Bioprinting of Thick Vascularized Tissues. *Proc. Natl. Acad. Sci. U. S. A.* **2016**, *113* (12), 3179–3184. https://doi.org/10.1073/pnas.1521342113.

(13) Choi, Y. J.; Jun, Y. J.; Kim, D. Y.; Yi, H. G.; Chae, S. H.; Kang, J.; Lee, J.; Gao, G.; Kong, J. S.; Jang, J.; Chung, W. K.; Rhie, J. W.; Cho, D. W. A 3D Cell Printed Muscle Construct with Tissue-Derived Bioink for the Treatment of Volumetric Muscle Loss. *Biomaterials* **2019**, *206* (October 2018), 160–169.

(14) Kim, B. S.; Das, S.; Jang, J.; Cho, D. W. Decellularized Extracellular Matrix-Based Bioinks for Engineering Tissue- And Organ-Specific Microenvironments. *Chem. Rev.* **2020**, *120* (19), 10608–10661. https://doi.org/10.1021/ACS.CHEMREV.9B00808/ASSET/IMAGES/LARGE/CR9B00808_0018.JPEG.

(15) Kim, H. H. K.; Jang, J.; Park, J.; Lee, K. P.; Lee, S.; Lee, D. M.; Kim, K. H.; Kim, H. H. K.; Cho, D. W. Shear-Induced Alignment of Collagen Fibrils Using 3D Cell Printing for Corneal Stroma Tissue Engineering. *Biofabrication* **2019**, *11* (3), 035017. https://doi.org/10.1088/1758-5090/AB1A8B.

(16) Prendergast, M. E.; Davidson, M. D.; Burdick, J. A. A Biofabrication Method to Align Cells within Bioprinted Photocrosslinkable and Cell-Degradable Hydrogel Constructs via Embedded Fibers. *Biofabrication* **2021**, *13* (4), 044108. https://doi.org/10.1088/1758-5090/ac25cc.

(17) Yongcong, F.; Zhang, T.; Liverani, L.; Boccaccini, A. R.; Sun, W. Novel Biomimetic Fiber Incorporated Scaffolds for Tissue Engineering. *J. Biomed. Mater. Res. - Part A* **2019**, *107* (12), 2694–2705. https://doi.org/10.1002/JBM.A.36773.

(18) Sydney Gladman, A.; Matsumoto, E. A.; Nuzzo, R. G.; Mahadevan, L.; Lewis, J. A. Biomimetic 4D Printing. *Nat. Mater.* **2016**, *15* (4), 413–418. https://doi.org/10.1038/nmat4544.

(19) Siqueira, G.; Kokkinis, D.; Libanori, R.; Hausmann, M. K.; Gladman, A. S.; Neels, A.; Tingaut, P.; Zimmermann, T.; Lewis, J. A.; Studart, A. R. Cellulose Nanocrystal Inks for 3D Printing of Textured Cellular Architectures. *Adv. Funct. Mater.* **2017**, *27* (12), 1604619. https://doi.org/10.1002/adfm.201604619.

(20) Espinosa, E.; Filgueira, D.; Rodríguez, A.; Chinga-Carrasco, G. Nanocellulose-Based Inks—Effect of Alginate Content on the Water Absorption of 3D Printed Constructs. *Bioengineering* **2019**, *6* (3), 65. https://doi.org/10.3390/bioengineering6030065.

(21) Shin, S.; Hyun, J. Matrix-Assisted Three-Dimensional Printing of Cellulose Nanofibers for Paper Microfluidics. *ACS Appl. Mater. Interfaces* **2017**, *9* (31), 26438–26446.

https://doi.org/10.1021/ACSAMI.7B07609/ASSET/IMAGES/LARGE/AM-2017-07609G_0006.JPEG.

(22) Shin, S.; Hyun, J. Rheological Properties of Cellulose Nanofiber Hydrogel for High-Fidelity 3D Printing. *Carbohydr. Polym.* **2021**, *263*, 117976. https://doi.org/10.1016/J.CARBPOL.2021.117976.

(23) de Nooy, A. E. J.; Besemer, A. C.; van Bekkum, H. Highly Selective Nitroxyl Radical-Mediated Oxidation of Primary Alcohol Groups in Water-Soluble Glucans. *Carbohydr. Res.* **1995**, *269* (1), 89–98. https://doi.org/10.1016/0008-6215(94)00343-E.

(24) Saito, T.; Isogai, A. TEMPO-Mediated Oxidation of Native Cellulose. The Effect of Oxidation Conditions on Chemical and Crystal Structures of the Water-Insoluble Fractions. *Biomacromolecules* **2004**, *5* (5), 1983–1989. https://doi.org/10.1021/bm0497769.

(25) Fukuzumi, H.; Saito, T.; Isogai, A. Influence of TEMPO-Oxidized Cellulose Nanofibril Length on Film Properties. *Carbohydr. Polym.* **2013**, *93* (1), 172–177. https://doi.org/10.1016/j.carbpol.2012.04.069.

(26) Tanaka, R.; Saito, T.; Ishii, D.; Isogai, A. Determination of Nanocellulose Fibril Length by Shear Viscosity Measurement. *Cellulose* **2014**, *21* (3), 1581–1589. https://doi.org/10.1007/s10570-014-0196-4.

(27) Yang, L.; Van Der Werf, K. O.; Koopman, B. F. J. M.; Subramaniam, V.; Bennink, M. L.; Dijkstra, P. J.; Feijen, J. Micromechanical Bending of Single Collagen Fibrils Using Atomic Force Microscopy. J. Biomed. Mater. Res. A 2007, 82 (1), 160–168. https://doi.org/10.1002/JBM.A.31127.

(28) Im, W.; Lee, S.; Rajabi Abhari, A.; Youn, H. J.; Lee, H. L. Optimization of

Carboxymethylation Reaction as a Pretreatment for Production of Cellulose Nanofibrils. *Cellulose* **2018**, *25* (7), 3873–3883.

(29) Pushpamalar, V.; Langford, S. J.; Ahmad, M.; Lim, Y. Y. Optimization of Reaction Conditions for Preparing Carboxymethyl Cellulose from Sago Waste. *Carbohydr. Polym.* **2006**, *64* (2), 312–318. https://doi.org/10.1016/j.carbpol.2005.12.003.

(30) Wågberg, L.; Decher, G.; Norgren, M.; Lindström, T.; Ankerfors, M.; Axnäs, K. The Build-up of Polyelectrolyte Multilayers of Microfibrillated Cellulose and Cationic Polyelectrolytes. *Langmuir* **2008**, *24* (3), 784–795. https://doi.org/10.1021/la702481v.

(31) Eyholzer, C.; Bordeanu, N.; Lopez-Suevos, F.; Rentsch, D.; Zimmermann, T.; Oksman, K. Preparation and Characterization of Water-Redispersible Nanofibrillated Cellulose in Powder Form. *Cellulose* **2010**, *17* (1), 19–30. https://doi.org/10.1007/s10570-009-9372-3.

(32) Bettadapur, A.; Suh, G. C.; Geisse, N. A.; Wang, E. R.; Hua, C.; Huber, H. A.; Viscio, A. A.; Kim, J. Y.; Strickland, J. B.; McCain, M. L. Prolonged Culture of Aligned Skeletal Myotubes on Micromolded Gelatin Hydrogels. *Sci. Rep.* **2016**, *6*, 28855. https://doi.org/10.1038/srep28855.

(33) Cakal, S. D.; Radeke, C.; Alcala, J. F.; Ellman, D. G.; Butdayev, S.; Andersen, D. C.; Calloe, K.; Lind, J. U. A Simple and Scalable 3D Printing Methodology for Generating Aligned and Extended Human and Murine Skeletal Muscle Tissues. *Biomed. Mater.* **2022**, *17* (4), 045013. https://doi.org/10.1088/1748-605X/AC6B71.

(34) Jensen, J. H.; Cakal, S. D.; Li, J.; Pless, C. J.; Radeke, C.; Jepsen, M. L.; Jensen, T. E.; Dufva, M.; Lind, J. U. Large-Scale Spontaneous Self-Organization and Maturation of Skeletal Muscle Tissues on Ultra-Compliant Gelatin Hydrogel Substrates. *Sci. Rep.* **2020**, *10* (1), 13305. https://doi.org/10.1038/s41598-020-69936-6.

(35) Choi, J. S.; Lee, S. J.; Christ, G. J.; Atala, A.; Yoo, J. J. The Influence of Electrospun Aligned Poly(Epsilon-Caprolactone)/Collagen Nanofiber Meshes on the Formation of Self-Aligned Skeletal Muscle Myotubes. *Biomaterials* **2008**, *29* (19), 2899–2906. https://doi.org/10.1016/J.BIOMATERIALS.2008.03.031.

(36) Wade, R. J.; Bassin, E. J.; Gramlich, W. M.; Burdick, J. A.; Wade, R. J.; Burdick, J. A.; Bassin, E. J.; Gramlich, W. M. Nanofibrous Hydrogels with Spatially Patterned Biochemical Signals to Control Cell Behavior. *Adv. Mater.* **2015**, *27* (8), 1356–1362. https://doi.org/10.1002/ADMA.201404993.

(37) Khodabukus, A.; Madden, L.; Prabhu, N. K.; Koves, T. R.; Jackman, C. P.; Muoio, D. M.; Bursac, N. Electrical Stimulation Increases Hypertrophy and Metabolic Flux in Tissue-Engineered Human Skeletal Muscle. *Biomaterials* **2019**, *198*, 259–269. https://doi.org/10.1016/j.biomaterials.2018.08.058.

(38) Miyamoto, K.; Tsuji, K.; Nakamura, T.; Tokita, M.; Komai, T. Preparation of Carboxymethyl-Gellan. *Carbohydr. Polym.* **1996**, *30* (2–3), 161–164. https://doi.org/10.1016/S0144-8617(96)00087-2.

(39) Engler, A. J.; Griffin, M. A.; Sen, S.; Bönnemann, C. G.; Sweeney, H. L.; Discher, D. E. Myotubes Differentiate Optimally on Substrates with Tissue-like Stiffness: Pathological Implications for Soft or Stiff Microenvironments. *J. Cell Biol.* **2004**, *166* (6), 877–887. https://doi.org/10.1083/jcb.200405004.

(40) Bhattacharyya, D.; Singhal, R. S.; Kulkarni, P. R. A Comparative Account of Conditions for Synthesis of Sodium Carboxymethyl Starch from Corn and Amaranth Starch. *Carbohydr. Polym.* **1995**, *27* (4), 247–253. https://doi.org/10.1016/0144-8617(95)00083-6.

(41) Nishino, T.; Takano, K.; Nakamae, K. Elastic Modulus of the Crystalline Regions of Cellulose Polymorphs. *J. Polym. Sci. Part B Polym. Phys.* **1995**, *33* (11), 1647–1651. https://doi.org/10.1002/polb.1995.090331110.

(42) McCain, M. L.; Agarwal, A.; Nesmith, H. W.; Nesmith, A. P.; Parker, K. K. Micromolded Gelatin Hydrogels for Extended Culture of Engineered Cardiac Tissues. *Biomaterials* **2014**, *35* (21), 5462–5471. https://doi.org/10.1016/j.biomaterials.2014.03.052.

(43) Gonzalez, G. M.; MacQueen, L. A.; Lind, J. U.; Fitzgibbons, S. A.; Chantre, C. O.; Huggler, I.; Golecki, H. M.; Goss, J. A.; Parker, K. K. Production of Synthetic, Para-Aramid and Biopolymer Nanofibers by Immersion Rotary Jet-Spinning. *Macromol. Mater. Eng.* **2017**, *302* (1), 1600365. https://doi.org/10.1002/mame.201600365.

(44) Dong, L.; Liang, M.; Guo, Z.; Wang, A.; Cai, G.; Yuan, T.; Mi, S.; Sun, W. A Study on Dual-Response Composite Hydrogels Based on Oriented Nanocellulose. *Int. J. Bioprinting* **2022**, *8* (3), 126–139. https://doi.org/10.18063/IJB.V8I3.578.

(45) Wang, X.; Chang, C. H.; Jiang, J.; Liu, Q.; Liao, Y. P.; Lu, J.; Li, L.; Liu, X.; Kim, J.; Ahmed, A.; Nel, A. E.; Xia, T. The Crystallinity and Aspect Ratio of Cellulose Nanomaterials Determine Their Pro-Inflammatory and Immune Adjuvant Effects In Vitro and In Vivo. *Small* **2019**, *15* (42). https://doi.org/10.1002/SMLL.201901642.

(46) Blaeser, A.; Filipa Duarte Campos, D.; Puster, U.; Richtering, W.; Stevens, M. M.; Fischer, H.; Blaeser, A.; Duarte Campos, D. F.; Puster, U.; Fischer, H.; Richtering, W.; Stevens, M. M. Controlling Shear Stress in 3D Bioprinting Is a Key Factor to Balance Printing Resolution and Stem Cell Integrity. *Adv. Healthc. Mater.* **2016**, *5* (3), 326–333. https://doi.org/10.1002/ADHM.201500677.

(47) Fonck, E.; Feigl, G. G.; Fasel, J.; Sage, D.; Unser, M.; Rüfenacht, D. A.; Stergiopulos, N. Effect of Aging on Elastin Functionality in Human Cerebral Arteries. *Stroke* **2009**, *40* (7), 2552–2556. https://doi.org/10.1161/STROKEAHA.108.528091.

TOC figure